

This is an Open Access document downloaded from ORCA, Cardiff University's institutional repository:<https://orca.cardiff.ac.uk/id/eprint/129855/>

This is the author's version of a work that was submitted to / accepted for publication.

Citation for final published version:

Selvarajoo, T., Davies, R. E. , Gardner, D. R. , Freeman, B. L. and Jefferson, A. D. 2020. Characterisation of a vascular self-healing cementitious material system: Flow and curing properties. *Construction and Building Materials* 245 , 118332. [10.1016/j.conbuildmat.2020.118332](https://doi.org/10.1016/j.conbuildmat.2020.118332)

Publishers page: <https://doi.org/10.1016/j.conbuildmat.2020.118332>

Please note:

Changes made as a result of publishing processes such as copy-editing, formatting and page numbers may not be reflected in this version. For the definitive version of this publication, please refer to the published source. You are advised to consult the publisher's version if you wish to cite this paper.

This version is being made available in accordance with publisher policies. See <http://orca.cf.ac.uk/policies.html> for usage policies. Copyright and moral rights for publications made available in ORCA are retained by the copyright holders.



# **CHARACTERISATION OF A VASCULAR SELF-HEALING CEMENTITIOUS MATERIAL SYSTEM: FLOW AND CURING PROPERTIES**

Selvarajoo T<sup>1</sup>, Davies RE<sup>1</sup>, Gardner DR<sup>1</sup>, Freeman BL<sup>1</sup>, Jefferson AD<sup>1\*</sup>

<sup>1</sup>School of Engineering, Cardiff University, Queen's Buildings, The Parade, Cardiff, CF24 3AA, UK

\*jeffersonad@cardiff.ac.uk

## **ABSTRACT**

A series of characterisation studies are reported that provide new data on the behaviour of a self-healing cementitious material (SHCM) system. A 'model' material system is selected for study that comprises cyanoacrylate (CA) filled channels in concrete structural elements. The focus of the work is on transport and curing properties of the healing-agent, with the results of four separate studies being presented. The experimental programme encompasses the capillary flow behaviour of CA in a static natural crack, the sorption of healing-agent through a cracked surface into a concrete specimen, the development and progress of a CA curing front adjacent to a concrete substrate and the dynamic flow characteristics of CA in capillary channels. A theoretical relationship is established for each of these processes, which allows meaningful parameters to be determined that help characterise the behaviour of the material system. In all cases, the processes were shown to have a significant degree of variability but, equally, to exhibit strong behavioural trends.

## **1. INTRODUCTION**

In recent years, self-healing cementitious materials (SHCMs) have received considerable attention from the civil engineering research community [1-3]. The motivation for this research effort undoubtedly arises from the fact that concrete cracking, and the ensuing durability problems, afflicts a significant number of concrete structures, both old and new, with the consequence that a large percentage of infrastructure spending is on the repair and maintenance of concrete structures [4].

A substantial number of SHCMs use encapsulated autonomic healing-agents [1-3]. These SHCMs have employed a number of different healing-agents and a range of methods for encapsulating, releasing and delivering those healing-agents to damage sites. The healing-agents used by previous investigators include polyurethane (PU) [5-10], sodium silicate [11-16], methyl-methacrylate [17-20], bacteria [16,21-23], epoxy resin [24-26] and cyanoacrylate [27-30]. Healing-agent storage and delivery techniques have comprised systems based on micro-encapsulation [12,20,26,31,32], macro-encapsulation [5,7,8,10,13,27,28] and embedded vascular networks [16,27,29,33-35].

Vascular networks have a number of advantages over some of the other delivering systems, such as their potential to continually supply an unlimited quantity of healing-agent to damage sites and their ability to be pressurised so as to boost the flow of healing-agent to cracked regions [16]. SHCM vascular systems have ranged from those that have isolated channels [27] to systems with more complex interconnected networks [35]. The network channels have been formed from cast-in glass tubes [27] or brittle 3D printed networks [35], as well as created by casting in and subsequently removing polymer tubes [33] or metal rods [34]. Sangadji and Schlangen [36] took an alternative approach and introduced networks of porous concrete in structural elements into which healing-agent could be injected.

The interested reader is referred to a number of review articles for a more complete account of the previous work on SHCMs [1-3,37-39].

Attention is now turned to previous work on the characterisation of the transport properties of SHCMs. It is noted that the characterisation of the mechanical properties of SHCMs is discussed in a linked paper [40].

A number of investigators have used the change in permeability of micro- and macro-cracked specimens as a measure of self-healing [5,6,22,41-45]. For example, Van Tittelboom et al. [5,22] used this approach to explore the healing efficiency of an encapsulation-based self-healing system. In their work, they formed single cracks in cylindrical specimens, which were then saturated with water using an established vacuum saturation technique [22]. The specimens were glued inside PVC rings, mounted in a test setup and then submerged in water on one side. These water permeability tests were used to measure the change in flow through discrete cracks before and after healing. The work was later extended to specimens with multiple cracks [6,7], although the authors concluded that their approach was far less effective in this case because of the difficulty of properly sealing all cracks.

Rather than employ pressurised flow, De Rooij et al. [46] investigated the healing efficiency of cracked mortar specimens using a capillary water absorption technique. The investigators used laboratory scale prismatic specimens (60mm x 60mm x 220mm), which were cracked and then oven-cured for 3 days. The specimens were then subjected to a sorptivity test in which the uptake of water through both the crack and surrounding matrix was measured. The results showed clear distinctions between healed and unhealed specimens, from which the authors concluded that this sorptivity test was an effective means of determining the degree of healing. A similar technique has also been used by a number of other investigators [11,47,48].

Yang et al. [20] used changes in gas permeability as a measure of healing in cementitious specimens with silica gel shell microcapsules containing methylmethacrylate monomer or triethylborane. The authors prepared a set of cylinder specimens ( $\varnothing$ 50mm x 100mm), cured for different periods (3 and 30 days), and then caused damage by subjecting them to a compressive load of 80% of their capacities. The specimens were then cut into 10mm thick cylindrical disk specimens, vacuum dried for 24 hours at room temperature, sealed and subjected to a gas permeability test. The authors reported reductions of 50.2% and 66.8% in the permeability of specimens that had healed for 3 and 30 days respectively.

The chloride penetration into a cementitious specimen has been used by several authors to assess the self-healing efficiency of different systems [31,48-50]. For example, Wang et al. [31] measured healing with respect to a chloride migration coefficient, which was calculated from the results of a rapid chloride-ion permeability test. The authors reported almost complete recovery of the chloride migration coefficient relative to that of the original material.

The crack filling properties of a PU-based healing-agent were investigated by Gilabert et al. [10]. In this work, the PU was encapsulated in borosilicate glass tubes that were subsequently glued into preformed holes in two concrete blocks. These blocks were then assembled to form a single specimen with a planar opening, which aimed to represent a crack, with the tubes bridging this opening. The assembled specimens were then subjected to direct tension loading. Their work included an evaluation of the proportion of a crack surface covered by the healing-agent -for a range of crack openings-, the measurement of the tensile strength of healed cracks and an evaluation of the fluid content of the capsules -before and after release- using  $\mu$ -CT imaging techniques. The authors also simulated the healing-agent flow using the computational fluid dynamics program OpenFOAM and found a reasonable agreement between the model predictions and their experimental observations. The change in the

healing-agent meniscus contact angle with time was also measured from the evolution of a polyurethane drop on a concrete substrate. It is noted that the velocity dependence of the contact angle was not reported in the paper.

Gardner et al. [51] presented a combined experimental and numerical study on the capillary flow of healing-agents within discrete planar openings in concrete specimens. The study included the investigation of the flow of cyanoacrylate through artificial planar cracks in concrete after 7 and 28 days of curing. A range of crack widths and crack configurations were considered, and the capillary rise response was measured. A modified Lucas-Washburn equation that allowed for stick-slip of the meniscus, frictional dissipation and wall slip was employed for the numerical simulation of the capillary flow. The work was extended in [52] in an investigation of the flow properties of cyanoacrylate and a GGBS solution. This work included the measurement of the capillary meniscus contact angles of the two liquid agents on different substrates, i.e. glass, saturated concrete and unsaturated concrete. In addition, the time viscosity relationship for these agents was established using a custom viscometer that comprised a concrete specimen with a cut horizontal rectangular channel, which was connected to transparent flexible tubes at either end of the channel. A time-dependent viscosity relationship, based on a momentum balance equation, was established for each healing-agent.

A very different type of approach was employed by Van Tittelboom et al. [53], who applied neutron radiography and tomography techniques to investigate the moisture distribution in self-healing cementitious materials. The above types of imaging can give useful insights into healing behaviour.

The above review illustrates that much of the previous research on SHCMs has been experimental in nature and has focused on developing and enhancing new cementitious self-healing materials, as well as on characterising the properties of various self-healing materials. Less attention has been paid to developing design procedures or numerical models for these materials, although some progress has been made on the latter [54]. As highlighted in reference [54], there has frequently been a mismatch between the data required for the development of a particular design or numerical model and the information available from existing experimental studies. This mismatch provided the primary motivation for the series of experiments reported in this paper. In this regard, four aspects of the curing and transport behaviour of healing-agents in an autonomic vascular system were identified as needing further investigation. These were i) the capillary flow of a healing-agent in a static natural crack; ii) the flow properties of a healing-agent through a cracked surface and in a micro-cracked region; iii) the curing kinetics of the healing-agent adjacent to a concrete substrate and iv) the dynamic flow properties of a healing-agent. The programme of work reported in this paper addresses each of these aspects for a selected vascular SHCM in which channels are embedded in concrete specimens (illustrated in Fig. 1).

The paper also describes a theoretical relationship for each of the processes, which allow meaningful parameters to be determined that help to characterise the material system.

The structure of the remainder of this paper is as follows;

- Section 2 provides the scope of the experimental programme and gives details of the materials used in the tests;
- Section 3 considers the capillary flow behaviour of CA in a static natural crack;
- Section 4 describes a set of experiments which determine the flow properties (or sorption characteristics) of a healing-agent through a cracked surface into a concrete specimen;
- Section 5 presents a set of tests designed to explore the existence and nature of a CA curing front with a concrete substrate;

- Section 6 describes a set of tests to determine the dynamic flow characteristics of CA in capillary channels;
- Section 7 gives some closing remarks.

## 2. SCOPE OF EXPERIMENTAL PROGRAMME

A significant number of SHCMs involve healing-agents being transported to damage sites, curing and then bonding with the surrounding matrix [1-3,37]. In some of these systems, the transport driving force is capillary pressure whilst in others pressurised networks are used [33]. Furthermore, in some scenarios, the damage and healing processes occur at different time scales but in other situations these processes overlap and interact. A comprehensive design procedure or numerical model for a SHCM system would encompass all of these situations; thus, the self-healing system and agent for the present experimental programme were chosen to cover all of these characteristics. This resulted in the choice of PC20 cyanoacrylate (CA) [55] as the healing-agent and a ‘vascular network’ as the healing system. The former was selected because it undergoes significant changes in its degree of cure in the time scale of a short-term laboratory test but equally CA does not fully heal a typical discrete crack (0.1 to 0.5mm in width) in negligible time relative to the time scale of such tests. To put this in context, results from mechanical direct tension tests with fixed crack healing periods (reported in the linked paper [40]) showed that significant healing (e.g. 40%) took place in a 0.1mm crack within the first 10 seconds but 300 seconds were required for the healing response to stabilise (i.e. for the healed strength and stiffness to reach plateau values), whilst in a 0.2mm crack, less healing had taken place within the first 10 seconds (e.g. 25%) and 1200 seconds were needed for stabilisation.

The choice of a ‘vascular network’, in which embedded channels are used to deliver healing-agent to discrete cracks, was made because it allows careful control over the delivery process and because it can be readily pressurised and monitored. The ‘model’ self-healing system, to which the present work relates, is illustrated in Fig. 1.

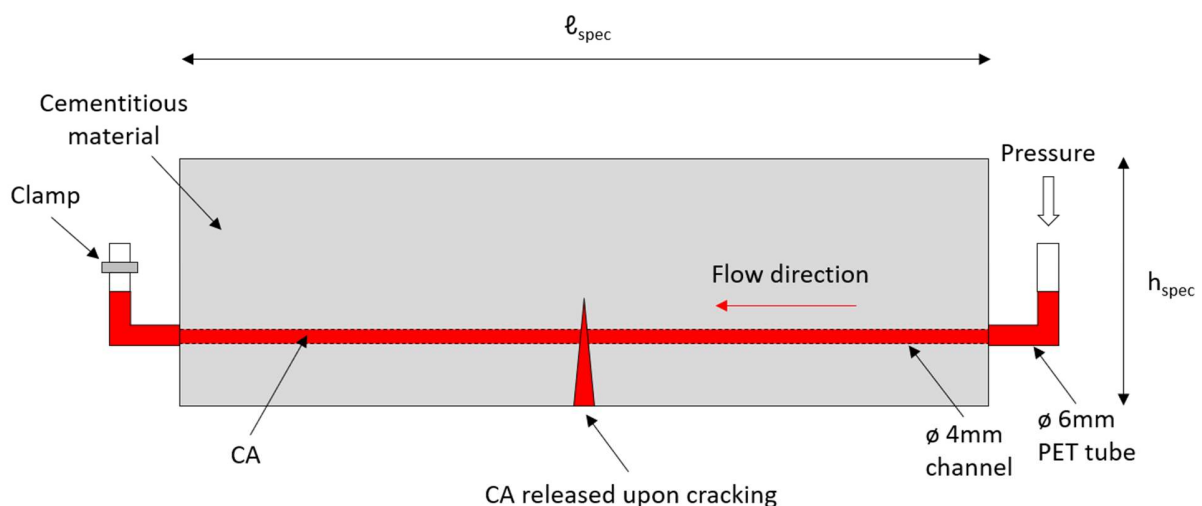


Fig. 1. Model self-healing system

The present experimental programme comprised the following series of tests.

**i. CA capillary flow in a static natural crack**

The flow characteristics of healing-agents under capillary pressure in natural cracks in concrete specimens is vital information for understanding and predicting the behaviour a vascular SH system. Previous work has considered the flow of various liquids in smooth sided openings (termed 'planar cracks') and natural cracks [51,52,56] but no results have previously been published on the flow of CA in natural cracks in concrete specimens. Such data are presented in this paper for a range of cracks in dry concrete specimens.

**ii. CA sorption tests**

When healing-agent flows into a discrete crack in a concrete specimen, a proportion of the fluid migrates into the matrix material adjacent to the crack. The region adjacent to a macro-crack in concrete generally contains micro-cracks and is part of the fracture process zone [57,58]. The sorption characteristics of this region are required to allow the proper simulation of the advective-diffusive flow of the healing-agent into and through this region. A series of tests were therefore undertaken to measure the uptake into a concrete specimen of CA through a crack face.

**iii. Curing front properties of CA with a concrete substrate**

There is a class of single component healing-agents, to which CA belongs, that cure via a polymerisation reaction. In the case of CA, this reaction is initiated by the presence of hydroxide ions [59-61] and may be considered effectively instantaneous with respect to the time scales considered in this study. Curing progresses as OH<sup>-</sup> ions diffuse through the body of CA and this process is significantly slower than the polymerisation reaction. It has been suggested that the polymerised material creates a barrier to further diffusion [61], which makes the progress of healing highly dependent on the width between the surfaces being bonded (i.e. the crack width in the present case). Data on this process, in relation to the curing of CA adjacent to a concrete body, were not previously available and therefore a series of experiments were undertaken to explore this process. The aim of these tests was to provide an indication of whether a curing front model is appropriate for the current self-healing system but no attempt was made to measure the curing rate of CA using such techniques as FTIR (Fourier-transform infrared spectroscopy), which has been undertaken by others, albeit with different substrates [61].

**iv. Dynamic flow characteristics of CA in capillary channels.**

When a healing-agent is pressurised in a vascular network, the flow velocity in a discrete crack can be sufficiently large for the meniscus to depart from its static configuration and for inertia forces to become non-negligible. It is generally accepted that the angle of contact between a moving meniscus and the adjacent substrate is velocity dependent [62]. This issue was studied in a series of tests in which CA was driven through a capillary tube using a pressurised flow system. The effects of using a glass, rather than concrete, substrate for these tests is addressed in detail in Section 6.2.

A set of theoretical models have been used to characterise the above tests and obtain meaningful parameters. The details of each of these models are provided in the relevant sections of the paper.

A standardised concrete mix with 10mm coarse aggregate was used to form the concrete specimens. Unless noted otherwise, these specimens were cast, demoulded at one day, cured under water for five days, dried in an oven at 90°C for 24 hours, allowed to cool to room temperature and then tested.

A specimen age of eight days was selected to facilitate a large experimental programme. Furthermore, provided the samples have the general properties and characteristics of hardened concrete, neither the absolute strength nor the degree of hydration was critical to the establishment of the autonomic self-healing characteristics. It is also worth mentioning that, at the selected temperature of 90°C, little or no thermal damage would be expected [63]. Furthermore, drying at this temperature minimises any potential interaction between the self-healing-agent and excess liquid capillary water.

The standard concrete mix used in these investigations is as follows;

Cement type: Ordinary Portland Cement (CEM II/A-L 32, 5R).

Coarse aggregate type: Crushed limestone.

Fine aggregate type: Crushed marine sand with limestone.

Mix proportions: 470 kg/m<sup>3</sup>: 728 kg/m<sup>3</sup>: 986 kg/m<sup>3</sup>: 216 kg/m<sup>3</sup> (cement: coarse aggregate: fine aggregate: water) with a maximum aggregate size of 10mm.

Slump: in accordance with BS EN 12350-2:2009.

Average (100mm) cube compressive strength ( $f_{cu}$ ): 39.4MPa with CoV of 5.2%.

Average cylinder (100x200mm) splitting tensile strength ( $f_{cyl}$ ): 3.4MPa with CoV of 10.2%.

It is generally accepted that the true tensile strength ( $f_t$ ) is approximately 0.85  $f_{cyl}$ , (i.e.  $f_t = 0.85 f_{cyl}$ ) and the true uniaxial strength ( $f_c$ ) is approximately 0.8  $f_{cu}$  (i.e.  $f_c = 0.8 f_{cu}$ ) [64].

### 3. CA CAPILLARY FLOW IN A STATIC NATURAL CRACK

Previous tests on the capillary flow of water in natural cracks and planar openings (i.e. openings with smooth surfaces), showed that there is a significant difference in capillary flow behaviour between these two cases [51,56]. Whilst some results have been published on the capillary flow characteristics of CA in planar openings, results on CA flow behaviour in natural rough cracks in concrete have not previously been presented.

In order to create naturally cracked specimens, a set of 75 x 75 x 255 mm prisms were cast using the standard concrete mix.

Due to the bonding nature of CA, only one test could be performed for each crack width. Natural cracks were created using seven-day old specimens. A 3mm wide, 7mm deep central notch was sawn into the lower face of all specimens and these were subsequently subjected to three-point bending and loaded to failure. Once the prisms were fully cracked, a pair of 45 x 75 x 25 mm specimens were cut from the central part of the cracked beam using a concrete cutting saw (which has a water-based dust suppressant system) and the resultant pieces, as shown in Fig. 2, were clamped together with spacers of appropriate thickness to create crack widths of 0.1mm, 0.2mm, and 0.3 mm.

The specimens, which had become damp during sawing, were subsequently dried in an oven for 12 hours.

A petri dish with CA was lifted to the underside of the clamped specimens using a hydraulic pump. The capillary flow was recorded using an AOS MOTIONeer high speed video camera with a capture rate of 250 frames per second. The camera was mounted on a platform 150mm in front of the specimens. To facilitate the measurement of the capillary rise, a scale rule was added to the front of the clamped specimens and adjustable lighting was used both in front and behind the specimens in order to illuminate the natural crack (see Fig. 3).

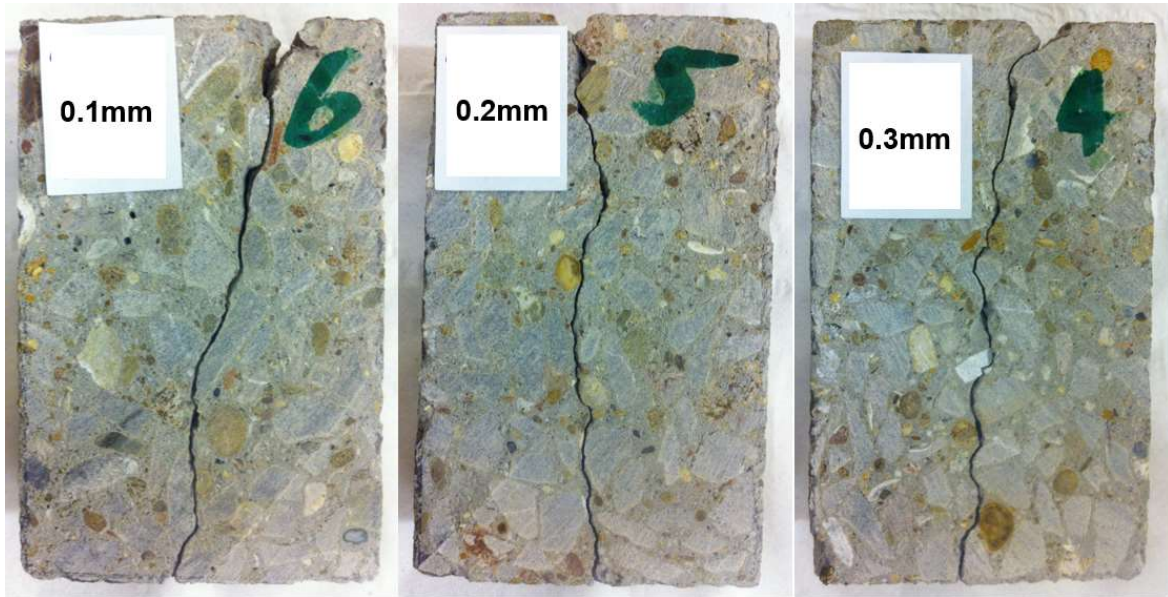


Fig. 2. Natural crack profiles for capillary rise investigation

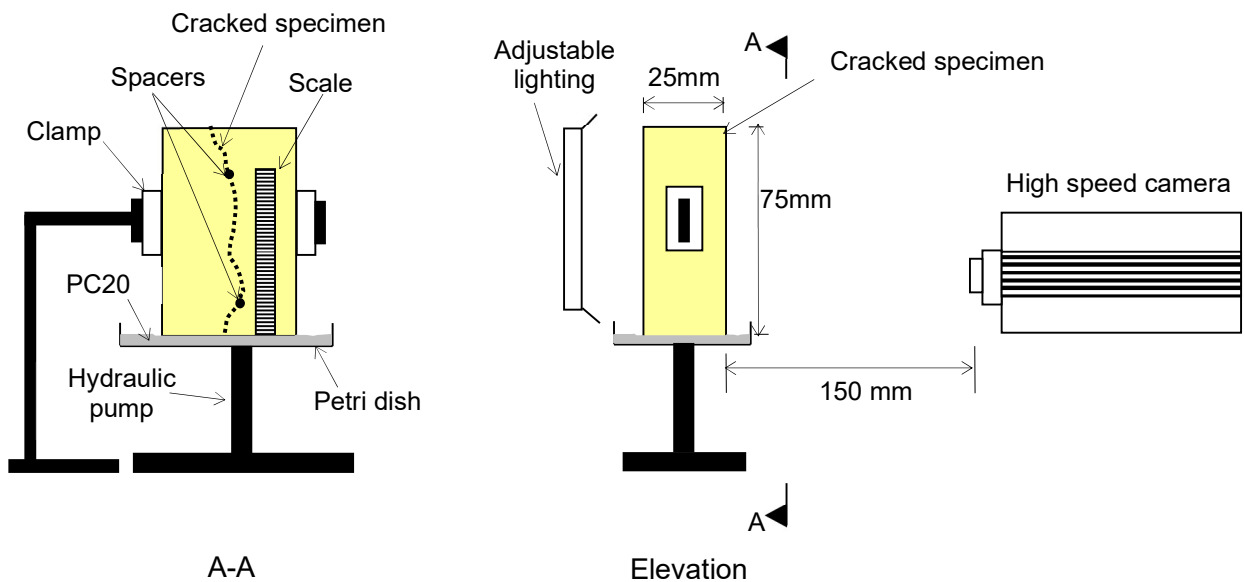


Fig. 3. Schematic sketch of the test setup

### 3.1 Capillary flow model

The capillary rise of the CA in the natural crack can be described using the modified Lucas-Washburn (LW) equation from Gardner et al. [51,52,56], which is given by:

$$\dot{z} = \frac{P_c(1 - \beta_s) - \rho g z \sin(\phi)}{\frac{2\beta_m}{w_c} + \eta} \quad (1)$$

where  $z$  represents the capillary rise height, the superior dot denotes a time derivative,  $w_c$  is the crack width,  $\phi$  is the angle of the flow channel measured from a vertical axis,  $\rho$  is the healing-agent density, and  $\beta_s$  and  $\beta_m$  are factors that account for stick-slip and frictional dissipation at the meniscus respectively [56].

The capillary pressure ( $P_c$ ) is given by the following Young-Laplace equation:

$$P_c = \frac{2\gamma \cos(\theta_d)}{w_c} \quad (2)$$

where  $\gamma$  is the capillary surface tension and  $\theta_d$  is the dynamic contact angle (DCA), which takes into account the departure of the contact angle from the equilibrium (or static) contact angle, with the movement of the meniscus. The characteristics of this behaviour are elaborated in Section 6 where a series of dynamic flow tests are presented.

The viscous resistance term ( $\eta$ ) is as follows;

$$\eta = w_c(z) \int_0^z \frac{1}{w_c(x) \left( \frac{w_c(x)\beta_w}{2} + \frac{k(x)}{\mu} \right)} dx \quad (3)$$

where  $x$  is an axial coordinate (0 to  $z$ ),  $\beta_w$  is a factor that accounts for wall slip [56] and the equivalent permeability term  $k = w_c^2/12$ .

### 3.2 Results and discussion

Post processing of the high-speed video recordings was completed using AOS Imaging Studio v3.6.6 and time-capillary rise height data were extracted. These data are shown in Fig. 4 for the three different crack openings along with the predictions from the numerical model. The latter are designated 'Num\_crack-opening', e.g. Num\_0.1mm relates to the numerical predictions for a crack opening of 0.1mm.

The specimens were examined 24 hours after testing and in all cases it was found that the two halves of the specimen were bonded together such that they could not be separated by hand. This observation does not provide a meaningful measure of the healed strength but it does indicate that the CA had cured to the point that no further flow was possible. It is noted that mechanical healing is addressed in a related publication [40].

The final capillary rise height, after a 24-hour period of curing and as observed on the exposed faces of the specimens once separated, averaged 8% higher than the height observed at the end of the recording period.

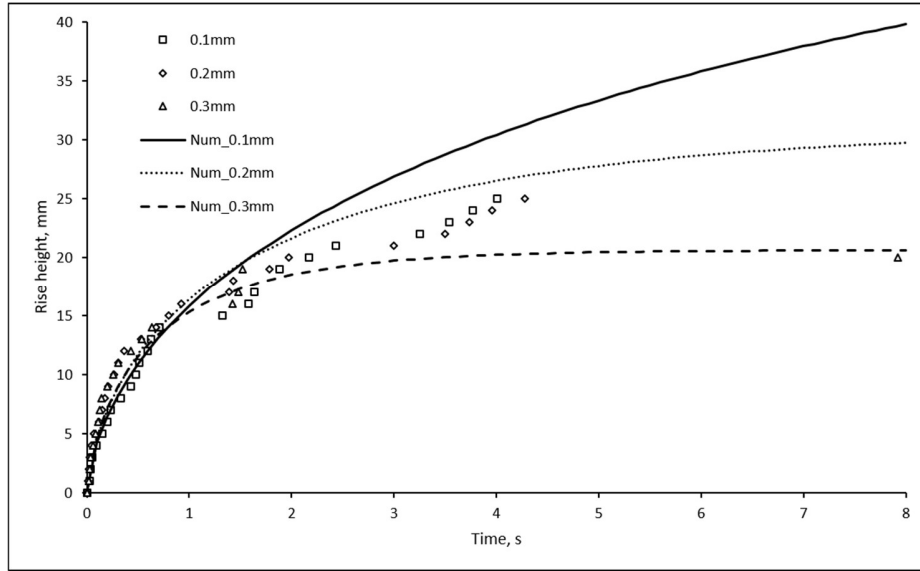


Fig. 4. Capillary rise height measurements in natural concrete cracks

Comparisons between a set of analytical results computed using equation (1) and the measured data are given in Fig. 4. The parameters derived from the model calibration are presented in Table 1.

Table 1. Calibrated parameters for crack flow test

Parameter	Value
$\beta_s$ (-)	0.01
$\beta_m$ (Ns/m <sup>2</sup> )	0.55
$\beta_w$ (m <sup>3</sup> /Ns)	0.0025

It can be seen from Fig. 4 that the capillary rise behaviour is captured reasonably well by this model, but that there are also some notable differences. An apparent discrepancy is that the experimental data show similar behaviour for the three different crack widths (from 0 to 4 seconds), whilst the model results suggest a stronger dependence on crack width. Although it is noted that the match between the experimental and numerical responses at 8 seconds, for the 0.3mm crack opening case, is close.

The trend found in these experimental results differs from that reported by Gardner et al. [51] for planar openings, which showed a more significant dependence on crack width throughout the rise time. It is believed that the differences between the behaviour of planar and natural cracks relate to the fact that in cracks with rough surfaces the crack opening varies considerably from the mean and that the tortuous nature of natural cracks (see Fig. 2) means that the actual flow path may be greater than the recorded rise height. In addition to this, cured CA may block (or form bridges between) the narrowest sections of the crack and a significant quantity of CA may flow through the crack walls into the concrete matrix. Considering further the issue of cured CA blocking the flow path; the morphology of natural crack surfaces is such that the slope of local surfaces around aggregate particles can be at sharp angles to the overall crack plane and geometry dictates that these local openings are far smaller than the average normal crack opening. It is known [55] that CA can cure rapidly (<5s) in small gaps (<0.05mm) and it is

believed that this type of rapid local curing occurs in the tests with all three openings. A wider opening would be required before these local openings in the tortuous path exceed 0.05mm. The authors believe that these CA bridges between opposing asperities form relatively early in the capillary rise tests and affect the results in terms of the rise response for a given crack opening.

#### 4. CA SORPTION TESTS

This study examined the sorption of CA into a concrete specimen through a natural crack surface. Notched prismatic specimens, which were formed from the standard concrete mix and which had the same dimensions as those described in Section 3, were used to create the test specimens. As in the tests described in Section 3, the specimens were loaded in three point bending to failure and then the two halves of the broken beam formed two separate sorption test specimens.

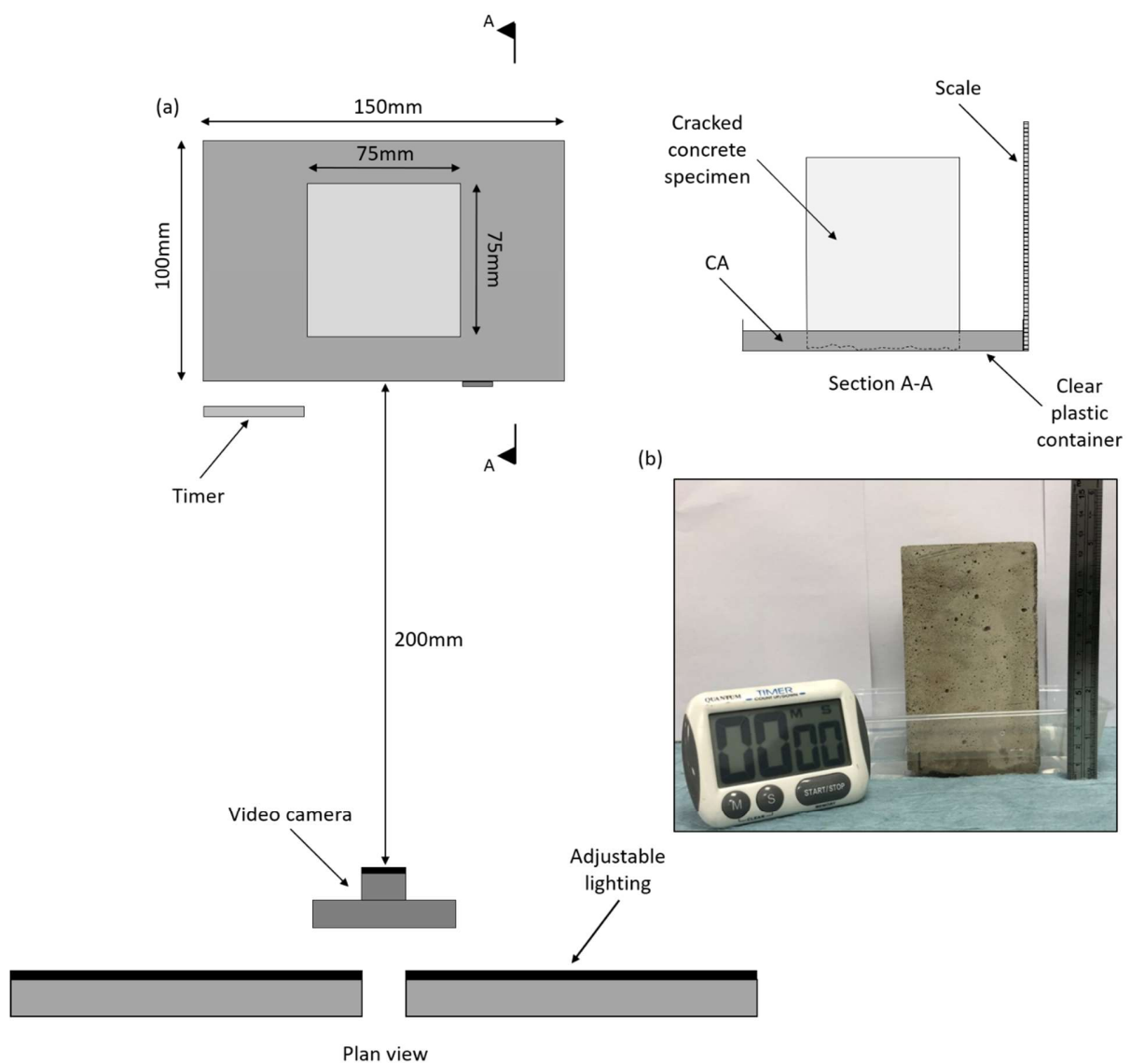


Fig. 5. (a) Schematic representation and (b) photograph of the test setup

The experimental test setup, illustrated in Fig. 5, comprised a shallow ‘bath’ (clear plastic container) of CA into which the specimen was placed, with the newly formed crack surface being placed vertically downwards and submerged in the CA pool. The sorption rise response was captured using a high-resolution digital video camera. A timer and a ruler were placed within the viewing frame and LED lights were used to illuminate the specimen. The digital recording was started prior to the concrete specimen being placed in the bath and continued for a period of 5 minutes from the time that the specimen first touched the surface of the CA bath. Preliminary tests had previously shown that the visible rise height reached a steady state in under five minutes.

#### 4.1 Sorption model

Unsaturated flow in a porous medium is described by the diffusive form of Richard’s equation, expressed as [65]:

$$\frac{\partial S_h}{\partial t} - \frac{\partial}{\partial x} \left( D(S_h) \frac{\partial S_h}{\partial x} \right) = 0 \quad (4)$$

in which  $S_h$  is the degree of healing-agent saturation,  $x$  is a vertical coordinate relative to the immersed surface,  $t$  is time and  $D(S_h)$  is a degree of saturation dependent diffusion function, which is given in the Appendix.

This equation can be solved numerically using a finite difference approximation, as shown in the Appendix, but an analytical solution may also be developed for the equation using Boltzmann’s transformation. Substituting the variable  $\lambda = xt^{-1/2}$  into equation (4), leads to the following ordinary differential equation:

$$-\frac{\lambda}{2} \frac{\partial S_h}{\partial \lambda} - \frac{\partial}{\partial \lambda} \left( D(S_h) \frac{\partial S_h}{\partial \lambda} \right) = 0 \quad (5)$$

Assuming a saturated boundary at the submerged face and an initially dry semi-infinite domain leads to the solution [65]:

$$x(S_h, t) = \lambda(S_h) t^{1/2} \quad (6)$$

The expression for cumulative volumetric absorption per unit area,  $i$ , is then expressed by [65,66]:

$$i = t^{1/2} \int_0^1 \lambda(S_h) dS_h = S t^{1/2} \quad (7)$$

where  $S$  is the sorptivity ( $\text{mm/s}^{1/2}$ ) of the material.

The volumetric absorption per unit area at time  $t$  can also be expressed as a function of the saturation profile:

$$i = \int_0^h S_h(x) dx \quad (8)$$

where  $h$  is the capillary rise height.

Following the approach of Hall and Hoff [66], eq. (7) is treated as a sharp front model and as such the material is assumed to be saturated behind the wetting front, giving the solution to eq. (8) as  $i = h$ .

In the present work, the rate of absorption is not constant and reduces as the CA cures and its viscosity increases. The rate of absorption is given by the differential of eq. (7), which is assumed linearly dependent on the degree of cure, and is expressed as follows (noting that  $i = h$ ):

$$\frac{\partial h}{\partial t} = (1 - \varphi(t)) \frac{S}{2} t^{-1/2} \quad (9)$$

The curing of CA adjacent to a cementitious substrate is discussed in detail in Section 5, in which it is shown that curing may be described with a curing front model that is governed by an exponential relationship for the propagation of the reaction front (eq. 11). Employing this approach to describe the curing of CA within the pore space, gives the expression for the degree of cure as  $\varphi(t) = 1 - e^{-t/\tau}$ , where  $\tau$  is a curing time parameter.

Integrating equation (9) and taking curing into account gives the following expression:

$$h = -\frac{\sqrt{\pi} S \operatorname{erfc}(\sqrt{t/\tau})}{2\sqrt{1/\tau}} + \frac{\sqrt{\pi} S}{2\sqrt{1/\tau}} \quad (10)$$

where  $\operatorname{erfc}(x)$  is the complimentary error function.

The above method is based on the assumption that there is a sharp moisture front. An alternative solution that makes no prior assumption about the nature of the moisture front is given in the Appendix.

## 4.2 Results and discussion

The processed results from the video files are presented in Fig. 6, in which the mean surface height of the CA, visible on the side of the specimen, is plotted against time. As CA flows into the specimen under capillary action, the specimen becomes darker in colour, and the upper limit of the darker section is interpreted as the internal limit of the CA.

It is acknowledged that this is an approximate method of determining the flow characteristics but, nevertheless, one that can be readily simulated using a continuum flow model in which the driving force is capillary suction [67].

The mean final rise height, from 4 specimens, was 3.1mm after 600 seconds with a CoV of 15%.

**Table 2.** CA sorption

Specimen	Weight change (g)	Glue uptake (ml)
S1	0.72	0.68
S2	0.52	0.49
S3	0.48	0.45
S4	0.54	0.51
<b>Mean</b>	0.56	0.53
<b>CoV (%)</b>	19	<b>19</b>

An attempt was made to determine the mass of CA absorbed by the specimen by weighing the samples immediately before and after the immersion period. After each test, the surfaces were wiped with a

damp cloth to remove excess CA but this did not prove easy due to the nature of CA. Therefore, the results presented in Table 2 are given with a degree of caution.

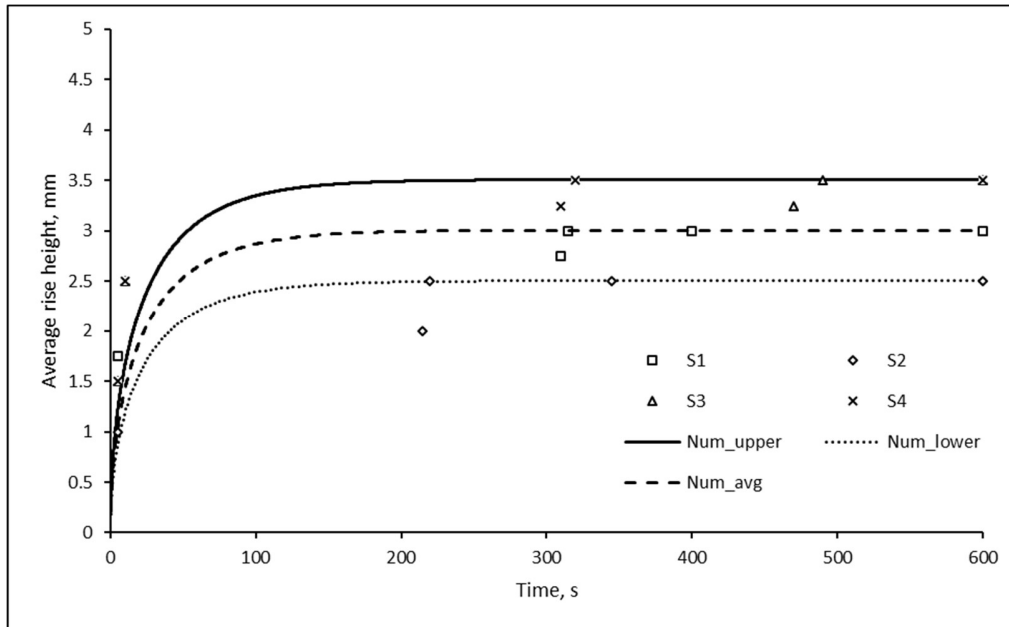


Fig. 6. Experimental and numerical sorption rise responses

Comparisons between the experimental results and analytical solutions are given in Fig. 6. The model was calibrated to match the upper bound, lower bound and average test responses, for which the parameters are given in Table 3. The sorption coefficient which gives the best match to the experimental data is  $S=0.48 \text{ mm/s}^{1/2}$ . The CoV of the sorption coefficients is 16.67 %.

Table 3. Calibrated model parameters for sorption test

Upper		Lower		Average	
Parameter	Value	Parameter	Value	Parameter	Value
$S(\text{mm/s}^{1/2})$	0.56	$S(\text{mm/s}^{1/2})$	0.40	$S(\text{mm/s}^{1/2})$	0.48
$\tau(\text{s})$	50	$\tau(\text{s})$	50	$\tau(\text{s})$	50

It can be seen from Fig. 6 that the average rise height is captured reasonably well by the sorption model.

## 5. CURING PROPERTIES OF CA WITH A CONCRETE SUBSTRATE

The objective of this set of experiments was to provide experimental evidence for the existence and nature of a curing front in CA with a concrete substrate. The tests rely on visual observations of a curing front and intermittent probes (an indenter) to check that the observed front relates to cured material (see Fig. 7).

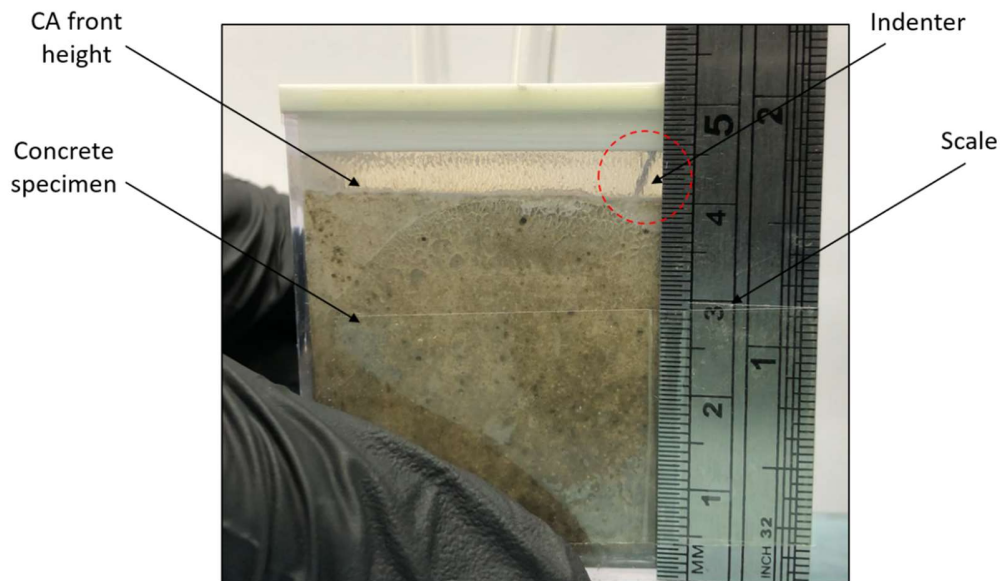


**Fig. 7.** Curing front test photograph, highlighting the indenter

The cracks considered in this programme of research are typically 0.1mm to 0.5mm in width and therefore curing front properties are required for a relatively narrow layer of healing-agent. It was therefore decided to use a small scale testing arrangement, as illustrated in Fig. 8, in which curing in a 6mm layer of CA above a 50mm cube of concrete material was observed.

The test procedure was as follows;

- Cubes of size 50mm x 50mm x 40mm were cast in a transparent Perspex box using the standard mix and curing regime (See Section 2);
- Once cured, the specimens were transferred to an identical (but clean) Perspex box, with clear silicone sealant used to seal the specimen and eliminate air gaps;
- The lids of the Perspex box were secured with CA to ensure air tightness;
- The gap above the specimen was then filled with CA using a syringe that passed through a hole in the lid: a second temporary breathing hole was introduced into the lid during filling;
- One hole was then sealed and the other was used for the indenter, which had an airtight seal;
- CA curing was then recorded with a digital camera for period of 30 minutes, with an indenter applied intermittently to verify that the visible curing front was being correctly interpreted.

It is noted that the test is assumed to start (i.e.  $t=0$ ), the moment that CA touches the substrate surface.

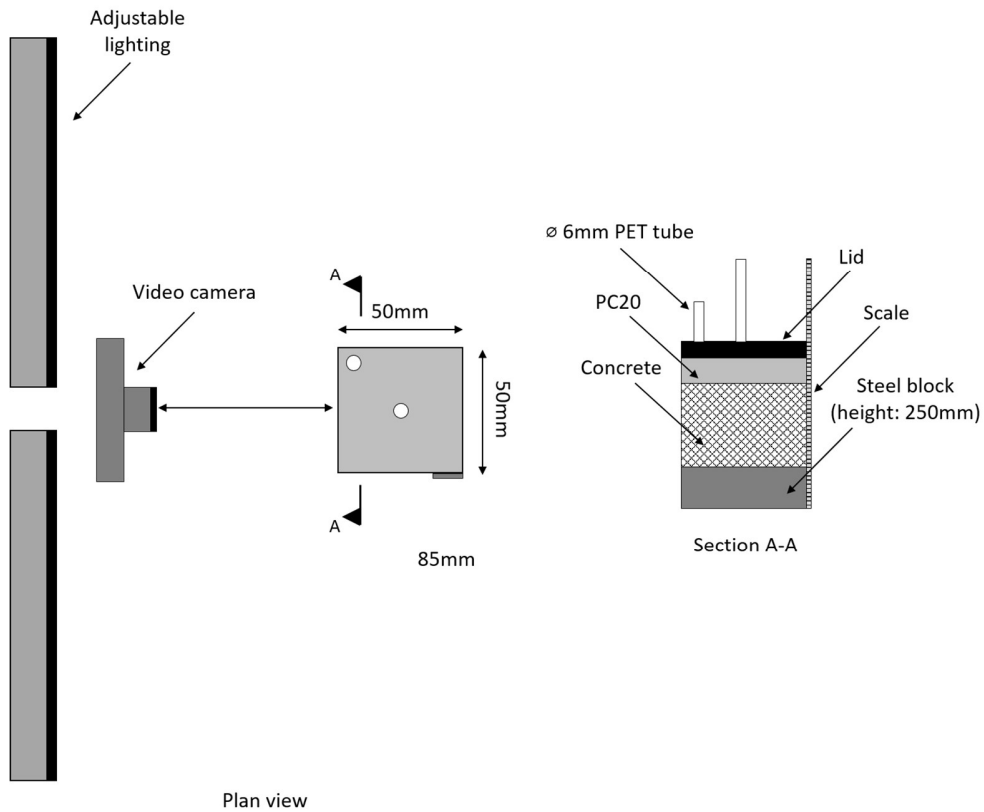


**Fig. 8.** Experimental setup

### 5.1 Curing front model

The curing of CA is a polymerisation reaction, initiated by hydroxide ions, which propagates into the glue from the substrate. Experimental evidence from Tomlinson et al. [61], as well as the data measured here, shows that the depth of cure of the CA tends towards a limiting value, after which no more curing occurs. This behaviour can be described by the following equation:

$$z_c(t) = z_{c0} \left( 1 - e^{-\frac{t}{\tau}} \right) \quad (11)$$

where  $z_c$  is the curing front position, relative to the substrate,  $z_{c0}$  is a critical curing depth and  $\tau$  is a curing time parameter.

### 5.2 Results and discussion

CA becomes opaque when it is cured and the limit of cured (opaque) material adjacent to the substrate is interpreted as the curing front, as illustrated in Fig. 9. For clarity, a dotted red line has been added to the figures to highlight the limit of the cured CA. The video images from all tests show that the front does not remain plane and parallel to substrate surface but becomes more irregular and increasingly diffuse over time.

Data extracted from the video images are presented in Fig. 10 in terms of curing front height (i.e. distance from substrate) versus time from the start of the experiment. The response suggests that the rate of progress of the curing front gradually diminishes over time.

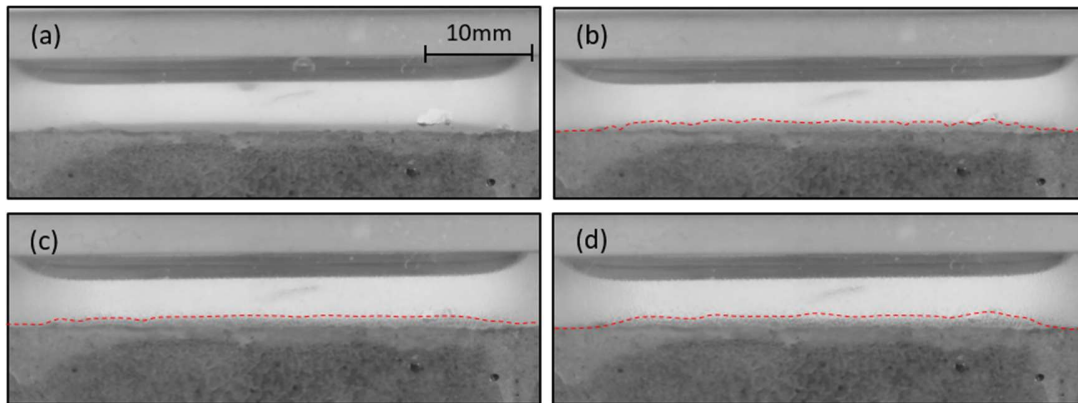


Fig. 9. Curing front of specimen at (a) 5 seconds, (b) 210 seconds, (c) 570 seconds and (d) 810 seconds

The model was calibrated to match the average response measured during the test, as illustrated in Fig. 10. In addition, in order to provide an indication of the sensitivity of the predicted response to the governing parameters, 'upper' and 'lower' numerical curves have also been added to the graph.

The parameters derived from this calibration exercise are given in Table 4.

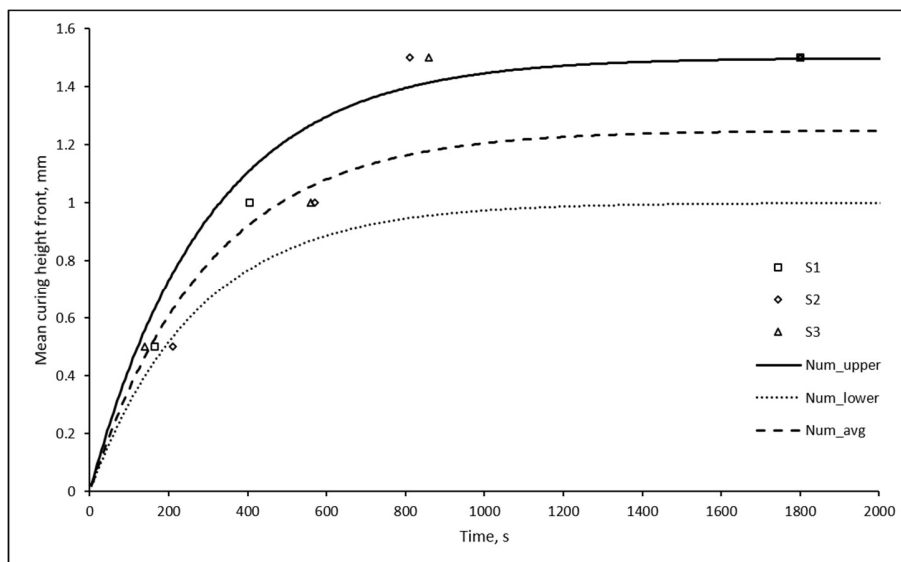


Fig. 10. Experimental and numerical mean curing front response

The spread of the experimental results shows that this process has a significant degree of variability and it is acknowledged that some judgement was required to discern the position of the front. Never-the-

less, these test results and observations do shed new light on the nature and behaviour of CA curing adjacent to a concrete substrate.

**Table 4.** Calibrated model parameters for curing front test

Upper		Lower		Average	
Parameter	Value	Parameter	Value	Parameter	Value
$z_{c0}$ (mm)	1.5	$z_{c0}$ (mm)	1	$z_{c0}$ (mm)	1.25
$\tau$ (s)	300	$\tau$ (s)	275	$\tau$ (s)	300

## 6. DYNAMIC FLOW CHARACTERISTICS OF CA IN CAPILLARY CHANNELS

This section reports a series of experimental studies on the flow of CA in a 0.3mm diameter glass capillary tube subjected to driving pressures of 0.1 bar, 0.3 bar, 0.5 bar and 1.0 bar. The dynamic flow behaviour was captured using a high-speed digital camera.

### 6.1 Preparation and testing

The testing arrangement, illustrated in Fig. 11, comprised CA in a glass capillary tube that was connected to an air-line via a pressure regulator. The CA and the gas pressure from the regulator were initially isolated from each other by a clamp. The test was illuminated with high intensity lighting, which was reflected from a matt-white board. The dynamic motion of the CA was captured using a Motion BLITZ Cube 2 high speed digital camera produced by Mickotron, which has a maximum resolution of 1280 x 1024 pixels. A recording speed of 3012 frames per second (fps) was selected and the shutter speed set to 51 $\mu$ s.

The regulator valve allowed different pressures to be applied and tests were carried out at pressures (at the regulator) of 0.1, 0.3, 0.5 and 1.0 bar.

The testing procedure was as follows;

- The capillary tube was cleaned and dried to remove any contaminants;
- A set of circular rings, perpendicular to the tube axis, were marked on the capillary tube at 10mm intervals ;
- The flexible supply tube was partially filled with CA and clamped to prevent flow;
- The flexible supply and exit tubes were then connected to the glass capillary tube;
- The air-line and regulator valve were connected to the flexible supply tube;
- The regulator was set to the appropriate pressure;
- The motion camera was activated and the clamp released to initiate flow;
- Once the CA front (i.e. the meniscus) had passed the camera's field of view, the flexible tube was re-clamped;
- After each test, the transient flow data and meniscus contact angle at the centre of the tube (i.e. position c in Fig. 11) were extracted.

Each glass capillary tube was used only once and each test (with the same parameters) was performed a minimum of three times. The static contact angle was measured in the horizontal tube with the fluid at

rest. This condition was induced by partially filling the glass tube with CA and then applying the clamp to prevent further flow.

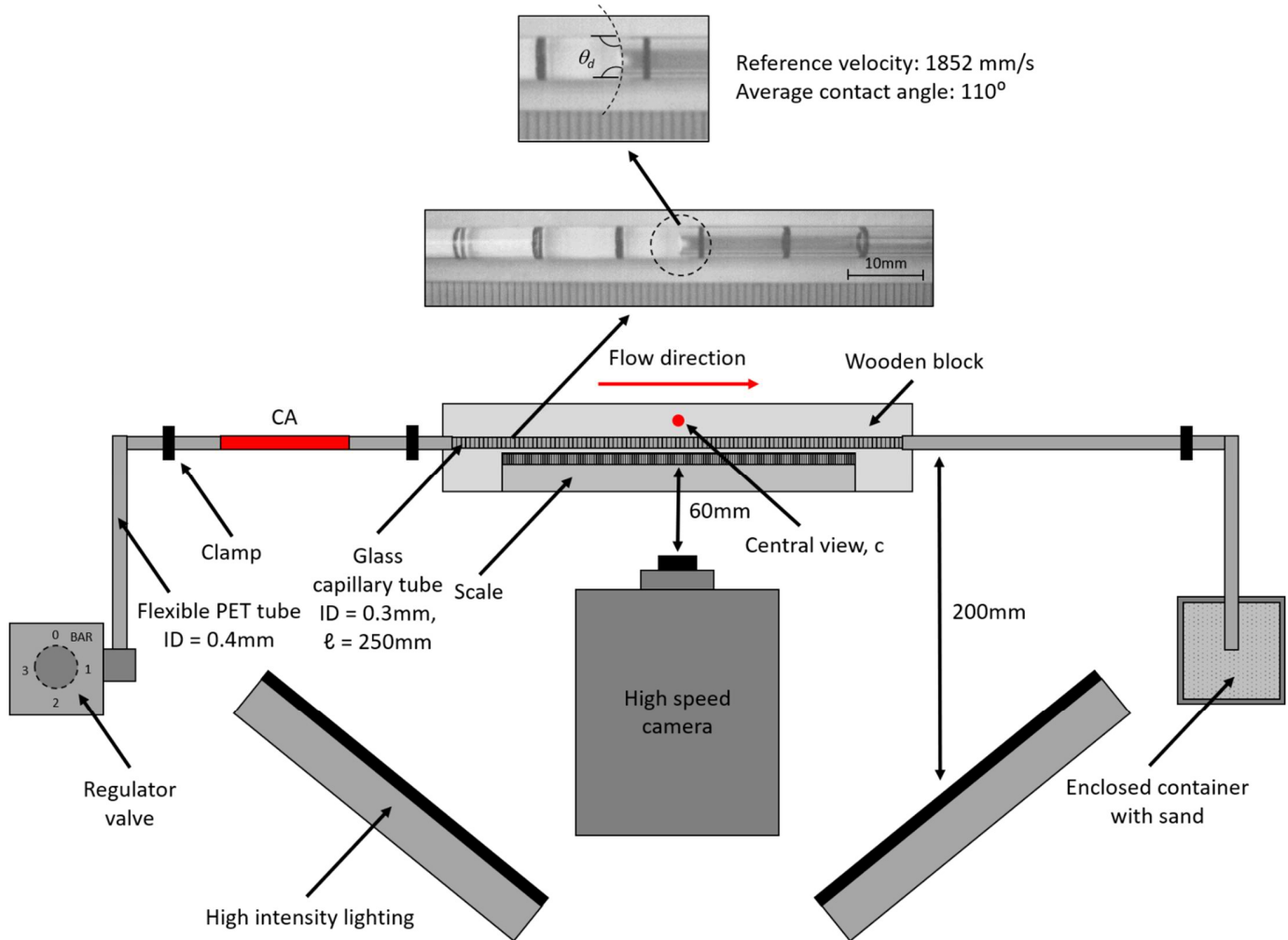


Fig. 11. Dynamic CA flow testing arrangement (plan view)

## 6.2 Dynamic contact angle model

Previous work on the dynamic flow behaviour of other liquids [62,68-70] suggests that the angle of contact ( $\theta_d$ ) between the liquid meniscus and the substrate depends on the flow velocity. A number of models have been developed for simulating dynamic capillary flow behaviour, including models by Jiang et al. [68], Bracke et al. [69] and Cox [70]. The relative merits of these and other models have been discussed by Blake [62]; however, we found that all three of these models provided very similar matches to the present experimental data. The empirically based formula of Bracke et al. [69], given in equation 12, was selected and calibrated for the present data.

$$\theta_d = \arccos(\cos\theta_s - C_1(1 + \cos\theta_s)C_a^{C_2}) \quad (12)$$

in which the capillary number  $C_a = \mu v / \gamma$ ;  $\mu$  is the dynamic viscosity ( $0.004 \text{ Ns/m}^2$ );  $v$  is the meniscus velocity (m/s);  $\gamma$  is the surface tension ( $0.034 \text{ N/m}$ );  $\theta_s$  is the static contact angle ( $37^\circ$ );  $\theta_d$  is the dynamic contact angle; and the constants  $C_1$  and  $C_2$  take the values is 0.8621 and 0.1947 respectively. In addition, the density ( $\rho$ ) of CA is  $1060 \text{ kg/m}^3$  [55].

### 6.3 Results and discussion

Transient capillary front graphs are presented for all tests in Fig. 12, which also gives the average velocity from each triplet of tests at the centre of the field of view (i.e. at the ‘reference velocity’). Some sample images from the experiment are given in Fig. 13, which shows the meniscus for both a static and a dynamic test.

As may be expected, the reference velocity increases with pressure. In addition, the flow approaches a steady-state velocity towards the time when the meniscus reaches the end of the field of view, which is indicated by the gradient of the flow-front graphs becoming linear.

There is considerable variation in the responses, with typical CoVs being 10%, but this is assumed to reflect the natural degree of variation of such dynamic flow processes.

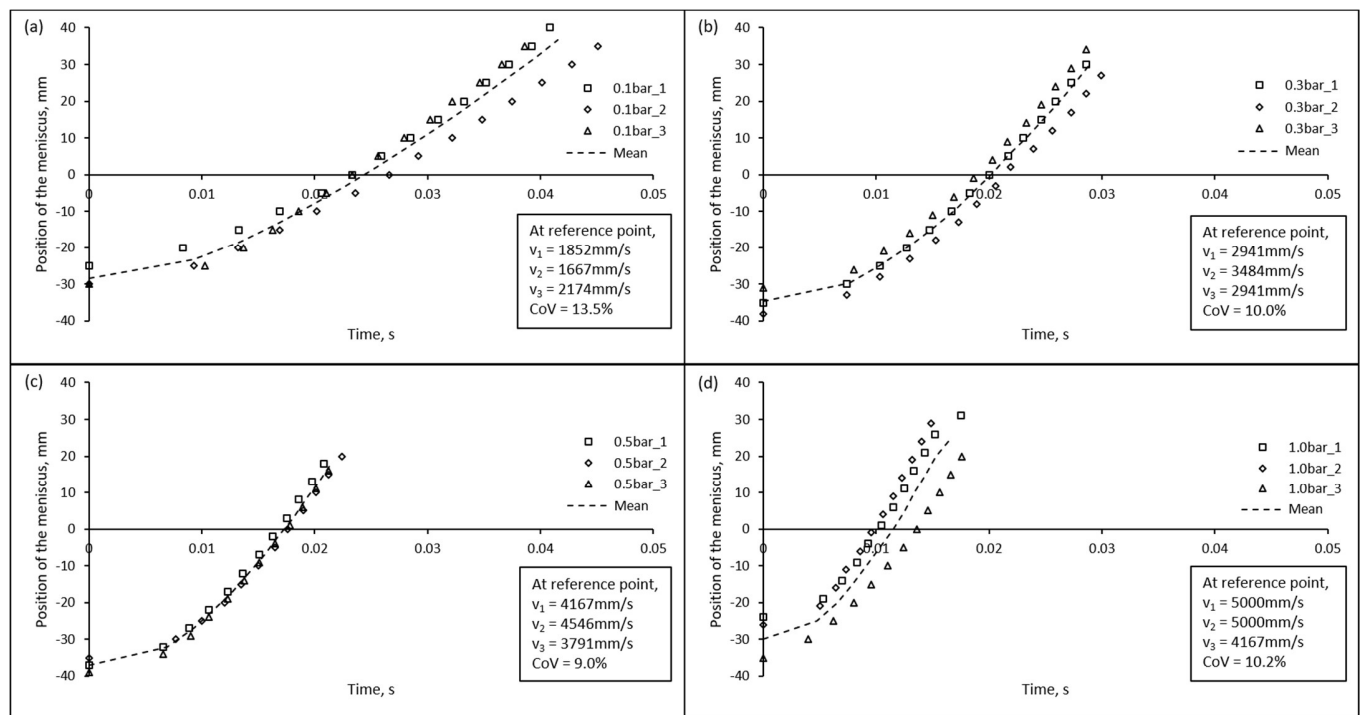


**Fig. 12.** Displacement - time responses at (a) 0.1bar, (b) 0.3bar, (c) 0.5bar and (d) 1.0bar of pressure

The contact angles have been extracted from the high-speed camera images using a technique developed by Stalder et al. [71]. These were calculated at different velocities and analysed when the meniscus reached the centre of the field of view. The CA contact angles were measured directly from

the wall of the glass capillary tube and these measurements were facilitated by the use of a plugin for the software ImageJ, called 'drop snake' [72].

From Fig. 13, it is apparent that the meniscus is asymmetric relative to a vertical plane, which is attributed to the effects of gravity. This, as may be expected, has a greater relative influence on static than dynamic behaviour since inertia forces are more dominant in the latter case.

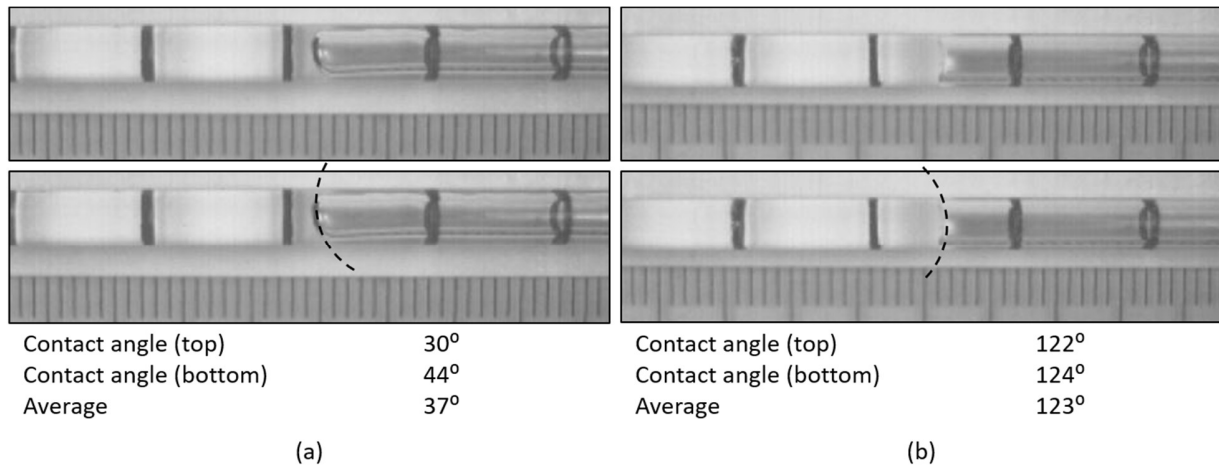


**Fig. 13.** ImageJ drop snake analysis for (a) static at 0mm/s velocity and (b) 0.5bar at 4546mm/s velocity

The processed data, in terms of  $\theta_d$  versus the meniscus velocity ( $v$ ), are presented in Fig. 14, which shows that there is a sharp transition from the low velocity region, for which the outer surface of the meniscus is concave ( $\theta_d < 90^\circ$ ), to a higher velocity region where the meniscus is convex ( $\theta_d > 90^\circ$ ). The transition point, corresponding to  $\theta_d = 90^\circ$ , is an important point in the curve, as when the meniscus becomes convex the surface tension retards, rather than drives, the flow. In all cases, the meniscus had become convex by the time it reached the reference position but the points at which the meniscus flipped from a concave to a convex shape were visible on the high-speed videos. However, because this abrupt transition occurred away from the centre of the field of view, the associated velocities were more difficult to determine accurately. Hence, the data points related to the transition (i.e. the points for  $\theta_d = 90^\circ$  on Fig. 14) are presented tentatively. The comparison between the DCA model (equation 12) and the current experimental data is given in Fig. 14.

It is recognised that these values are for CA with a glass substrate whereas in the self-healing material system the substrate is concrete. This was necessary as cementitious materials are not transparent and current imaging techniques do not allow such high-speed images to be captured accurately through opaque materials. The contact angle formed between any given fluid and a substrate depends on the surface roughness and chemical composition of the substrate [73]. The contact angle can therefore be expected to be different for CA-concrete than the measured CA-glass. However, Schwartz and Tejada [74] found that surface roughness had no significant effect on predictions with a DCA model, provided that the roughness is random and that the physiochemical character of the surfaces is similar. Whilst Seebergh and Berg [75] found that, for low capillary numbers, surface roughness produced significant stick-slip effects, but did not alter the constants in a DCA model, and that the static contact angle adequately accounts for the effect of acid-base (chemical) interactions. In the present work, therefore,

the differences in substrate are addressed by adjusting the static contact angle,  $\theta_s$ , using previously measured CA-concrete contact angle data [52].

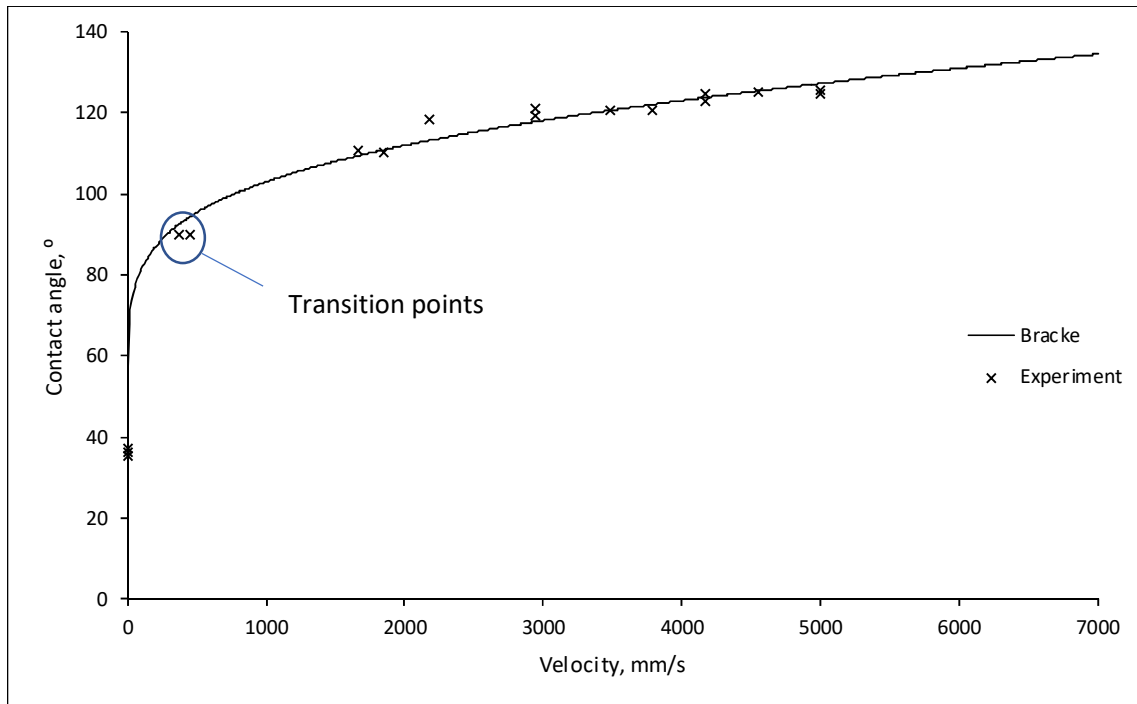


Fig. 14. Dynamic contact angle data

## 7. CLOSING REMARKS

This study has provided new data and new insights into the transport behaviour of CA in concrete specimens in the context of a vascular self-healing material system.

New data are presented on the capillary flow characteristics of CA in a natural concrete crack. These data show the effect of varying the crack width on the capillary rise response. It is notable that the change in response over the crack width range considered (0.1 to 0.3mm) is considerably less marked than that in planar (smooth-sided) openings [51]. The study also showed that the modified Lucas-Washburn equation proposed by Gardner et al. [56] is able to provide a reasonable match to the experimental response, although the need to account for the change of properties due to curing and to allow for the loss of CA into the concrete matrix has been highlighted. It is also noted that these two factors have been taken into account in linked modelling work.

The sorption of liquid CA through a crack wall in a concrete specimen has been measured in order to determine the loss of CA from the crack domain into the concrete matrix. This process was shown to have a reasonable degree of variability (i.e. CoV of a sorption constant = 16.67 %). It has also been shown that a simple sorption model is able to satisfactorily simulate the full sorption process when curing is taken into account.

The nature of CA curing with a concrete substrate has been determined. It was shown that a discernible curing front develops adjacent to the substrate wall and that this progresses over time but gradually

becomes less planar and more diffuse. The rate of progress of the front was shown to gradually reduce and this was attributed to the fact that cured CA provides an increasingly wide barrier to the source of hydroxide ions, which need to be present for curing to take place [61]. It was further shown that the progress of the curing front could be well represented by an exponential relationship but that the process is again relatively variable (e.g. the CoV of a primary curing front constant is 20 %).

The final experimental test investigated the dynamic flow characteristics of CA in a capillary channel and a relationship was established for the velocity dependency of the dynamic contact angle. It should be mentioned that this study is linked to previous work [52] in which the effects of curing on CA flow characteristics were measured.

The new data presented in this paper provided useful information for the development and validation of a coupled numerical model for vascular self-healing systems, described in reference [76], and hopefully will be useful to others working on the development of self-healing materials.

## APPENDIX

In the present work, the numerical solution of Equation (4) employs a backwards in time central in space finite difference scheme for the temporal and spatial discretisation, which leads to:

$$-\gamma S_{h,i+1}^{t+1,k+1} + (2\gamma + 1)S_{h,i}^{t+1,k+1} - \gamma S_{h,i-1}^{t+1,k+1} = S_{h,i}^{t,k} \quad (13)$$

where  $\gamma = D_i^{k+1}(S_{h,i}^{t+1,k}, t) \Delta t / \Delta x^2$ ,  $i$  denotes the node number,  $t$  the time step number and  $k$  the iteration number. The dependence of the diffusion coefficient is described by the expression presented in [77], which, adding terms to account for the effect of the degree of cure, is given by:

$$D(S_h, t) = D_1 \left( \alpha + \frac{1 - \alpha}{1 + \left( \frac{1 - S_h}{1 - S_{hc}} \right)^n} \right) (1 - \varphi(t)) \quad (14)$$

in which  $D_1$  is the diffusivity at saturation,  $S_{hc} = 0.8$  is the degree of saturation at which  $D(S_h) = 0.5D_1$ ,  $\alpha = 0.05$  and  $n = 15$ .

Comparisons between the experimental data and numerical solutions are given in Fig. 15. The numerical solutions were based on the assumption that the position of the moisture front corresponds to a degree of saturation of 0.6, which was chosen after some separate modelling exercises. The time step size was chosen as  $\Delta t = 0.1s$ , whilst the grid step size was chosen as  $\Delta x = 0.05mm$ . The model parameters are given in Table 5. The diffusion coefficient which gives the closest match to the experimental data is  $D_I = 7 \text{ mm}^2/s$ . The CoV of the diffusion coefficients is 32.89 %.

**Table 5.** Calibrated model parameters for sorption test

Upper		Lower		Average	
Parameter	Value	Parameter	Value	Parameter	Value
$D_I$ (mm <sup>2</sup> /s)	9.75	$D_I$ (mm <sup>2</sup> /s)	5	$D_I$ (mm <sup>2</sup> /s)	7
$\tau$ (s)	40	$\tau$ (s)	40	$\tau$ (s)	40

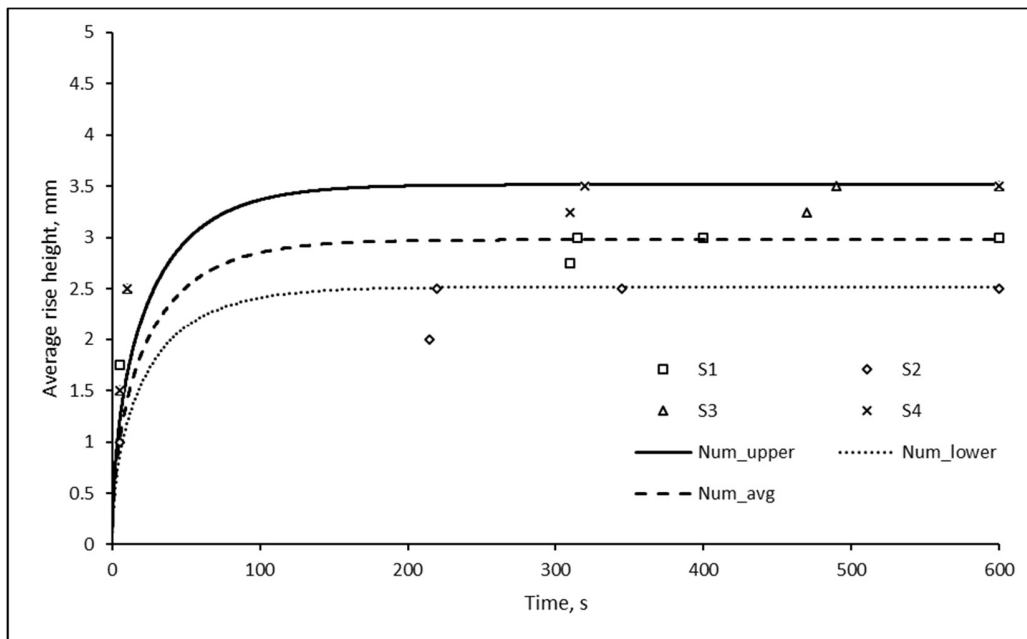


**Fig. 15.** Comparison between theoretical and experimental data

It can be seen from Fig. 15 that the average rise height is captured well by the diffusion model.

## ACKNOWLEDGEMENTS

The authors primarily acknowledge the financial support from the Engineering and Physical Sciences Research Council (EPSRC) research grant EP/P02081X/1, Resilient Materials for Life (<http://RM4L.com/>) under which the majority of the work was undertaken but also mention a previous research grant EP/J021776/1.

In addition, we acknowledge the support of other members of the M4L research group and make particular mention of the excellent technical assistance received from the laboratory staff at the Cardiff School of Engineering, especially from Ian King and Richard Thomas.

Information on the data underpinning the results presented here, including how to access them, can be found in the Cardiff University data catalogue at (<http://doi.org/10.17035/d.2019.0081928129>).

## REFERENCES

- [1] K. Van Tittelboom, N. De Belie, Self-healing in cementitious materials-a review, (2013). doi:10.3390/ma6062182.
- [2] M.M. Borah, N. Chetia, A Review on Self Healing Concrete, *Int. Conf. Adv. Mater. Tech.* - 2016. (2016). doi:10.5923/j.jce.20150503.01.
- [3] N. De Belie, E. Gruyaert, A. Al-Tabbaa, P. Antonaci, C. Baera, D. Bajare, A. Darquennes, R. Davies, L. Ferrara, T. Jefferson, C. Litina, B. Miljevic, A. Otlewska, J. Ranogajec, M. Roig-Flores, K. Paine, P. Lukowski, P. Serna, J.M. Tulliani, S. Vucetic, J. Wang, H.M. Jonkers, A Review of Self-Healing Concrete for Damage Management of Structures, *Adv. Mater. Interfaces*. 5 (2018) 1–28. doi:10.1002/admi.201800074.
- [4] D. Gardner, R. Lark, T. Jefferson, R. Davies, A survey on problems encountered in current concrete construction and the potential benefits of self-healing cementitious materials, *Case Stud. Constr. Mater.* 8 (2018) 238–247. doi:10.1016/j.cscm.2018.02.002.
- [5] K. Van Tittelboom, N. De Belie, D. Van Loo, P. Jacobs, Self-healing efficiency of cementitious materials containing tubular capsules filled with healing-agent, *Cem. Concr. Compos.* 33 (2011) 497–505. doi:10.1016/j.cemconcomp.2011.01.004.
- [6] K. Van Tittelboom, E. Tsangouri, D. Van Hemelrijck, N. De Belie, The efficiency of self-healing concrete using alternative manufacturing procedures and more realistic crack patterns, *Cem. Concr. Compos.* 57 (2015) 142–152. doi:10.1016/j.cemconcomp.2014.12.002.
- [7] K. Van Tittelboom, J. Wang, M. Araújo, D. Snoeck, E. Gruyaert, B. Debbaut, H. Derluyn, V. Cnudde, E. Tsangouri, D. Van Hemelrijck, N. De Belie, Comparison of different approaches for self-healing concrete in a large-scale lab test, *Constr. Build. Mater.* 107 (2016) 125–137. doi:10.1016/j.conbuildmat.2015.12.186.
- [8] M. Maes, K. Van Tittelboom, N. De Belie, The efficiency of self-healing cementitious materials by means of encapsulated polyurethane in chloride containing environments, *Constr. Build. Mater.* 71 (2014) 528–537. doi:10.1016/j.conbuildmat.2014.08.053.
- [9] J. Feiteira, E. Tsangouri, E. Gruyaert, C. Lours, G. Louis, N. De Belie, Monitoring crack movement in polymer-based self-healing concrete through digital image correlation, acoustic emission analysis and SEM in-situ loading, *Mater. Des.* 115 (2017) 238–246. doi:10.1016/j.matdes.2016.11.050.
- [10] F.A. Gilabert, K. Van Tittelboom, J. Van Stappen, V. Cnudde, N. De Belie, W. Van Paeppegem, Integral procedure to assess crack filling and mechanical contribution of polymer-based healing-agent in encapsulation-based self-healing concrete, *Cement and Concrete Composites*. 77 (2017) 68-80
- [11] R. Alghamri, A. Kanellopoulos, A. Al-Tabbaa, Impregnation and encapsulation of lightweight aggregates for self-healing concrete, *Constr. Build. Mater.* 124 (2016) 910–921. doi:10.1016/j.conbuildmat.2016.07.143.
- [12] A. Kanellopoulos, P. Giannaros, D. Palmer, A. Kerr, A. Al-Tabbaa, Polymeric microcapsules with switchable mechanical properties for self-healing concrete: synthesis, characterisation and proof of concept, *Smart Mater. Struct.* 26 (4) (2017) 045025. doi:10.1088/1361-665X/aa516c.

- [13] A. Formia, S. Irico, F. Bertola, F. Canonico, P. Antonaci, N.M. Pugno, J.M. Tulliani, Experimental analysis of self-healing cement-based materials incorporating extruded cementitious hollow tubes. *Journal of Intelligent Material Systems and Structures* 27 (2016) 2633–2652. doi:10.1177/1045389X16635847.
- [14] H. Mihashi, Y. Kaneko, T. Nishiwaku, K. Otsuka, Fundamental study on development of intelligent concrete characterized by self-healing capability for strength, *Trans. Jpn Concr. Inst.* 22 (2000) 441-450.
- [15] E. Mostavi, S. Asadi, M.M. Hassan, M. Alansari, Evaluation of self-healing mechanisms in concrete with double-walled sodium silicate microcapsules, *J. Mater. Civ. Eng.* (2015). p. 04015035.
- [16] R. Davies, O. Teall, M. Pilegis, A. Kanellopoulos, T. Sharma, A. Jefferson, D. Gardner, A. Al-Tabbaa, K. Paine, R. Lark, Large Scale Application of Self-Healing Concrete: Design, Construction, and Testing, *Front. Mater.* 5 (2018) 1–12. doi:10.3389/fmats.2018.00051.
- [17] C. Dry, Matrix cracking repair and filling using active and passive modes for smart timed release of chemicals from fibers into cement matrices, *Smart Mater. Struct.* 3 (1994) 118–123. doi:10.1088/0964-1726/3/2/006.
- [18] C. Dry, W. McMillan, Three-part methylmethacrylate adhesive system as an internal delivery system for smart responsive concrete, *Smart Mater. Struct.* 5 (1996) 297–300. doi:10.1088/0964-1726/5/3/007.
- [19] K. Van Tittelboom, K. Adesanya, P. Dubruel, P. Van Puyvelde, N. De Belie, Methyl methacrylate as a healing-agent for self-healing cementitious materials, *Smart Mater. Struct.* 20 (2011). doi:10.1088/0964-1726/20/12/125016.
- [20] Z. Yang, J. Hollar, X. He, X. Shi, A self-healing cementitious composite using oil core/silica gel shell microcapsules, *Cem. Concr. Compos.* 33 (2011) 506–512. doi:10.1016/j.cemconcomp.2011.01.010.
- [21] H. Jonkers, A. Thijssen, G. Muyzer, O. Copuroglu, E. Schlangen. Application of bacteria as self-healing-agent for the development of sustainable concrete. *Ecological Engineering* 36 (2010) 230-235
- [22] K. Van Tittelboom, N. De Belie, W. De Muynck, W. Verstraete, Use of bacteria to repair cracks in concrete, *Cem. Concr. Res.* 40 (2010) 157–166. doi:10.1016/j.cemconres.2009.08.025.
- [23] J. Wang, K. Van Tittelboom, N. De Belie, W. Verstraete, Use of silica gel or polyurethane immobilized bacteria for self-healing concrete, *Constr. Build. Mater.* 26 (2012) 532–540. doi:10.1016/j.conbuildmat.2011.06.054.
- [24] Q. Li, Siddaramaiah, N.H. Kim, D. Hui, J.H. Lee, Effects of dual component microcapsules of resin and curing agent on the self-healing efficiency of epoxy, *Compos. Part B Eng.* 55 (2013) 79–85. doi:10.1016/j.compositesb.2013.06.006.
- [25] W. Li, Z. Jiang, Z. Yang, Acoustic characterization of damage and healing of microencapsulation-based self-healing cement matrices, *Cem. Concr. Compos.* 84 (2017) 48–61. doi:10.1016/j.cemconcomp.2017.08.013.
- [26] G. Perez, E. Erkizia, J.J. Gaitero, I. Kaltzakorta, I. Jiménez, A. Guerrero, Synthesis and characterization of epoxy encapsulating silica microcapsules and amine functionalized silica nanoparticles for development of an innovative self-healing concrete, *Mater. Chem. Phys.* 165 (2015) 39–48. doi:10.1016/j.matchemphys.2015.08.047.

- [27] C. Joseph, A.D. Jefferson, B. Isaacs, R. Lark, D. Gardner, Experimental investigation of adhesive-based self-healing of cementitious materials, *Mag. Concr. Res.* 62 (2010) 831–843. doi:10.1680/mac.2010.62.11.831.
- [28] V.C. Li, Y.M. Lim, Y.W. Chan, Feasibility study of a passive smart self-healing cementitious composite, *Compos. Part B Eng.* 29 (1998) 819–827. doi:10.1016/S1359-8368(98)00034-1.
- [29] L. Sun, W. Yu, Q. Ge, Experimental research on the self-healing performance of micro-cracks in concrete bridge, *Adv. Mater. Res.* 250 (2011) 28-32.
- [30] H. Huang, G. Ye, Z. Shui, Feasibility of self-healing in cementitious materials - By using capsules or a vascular system?, *Constr. Build. Mater.* 63 (2014) 108–118. doi:10.1016/j.conbuildmat.2014.04.028.
- [31] X. Wang, F. Xing, M. Zhang, N. Han, Z. Qian, Experimental study on cementitious composites embedded with organic microcapsules, *Materials (Basel)*. 6 (2013) 4064–4081. doi:10.3390/ma6094064.
- [32] L. Souza, A. Al-Tabbaa, Microfluidic fabrication of microcapsules tailored for self-healing in cementitious materials, *Constr. Build. Mater.* 184 (2018) 713–722. doi:10.1016/j.conbuildmat.2018.07.005.
- [33] R. Davies, A. Jefferson, R. Lark, D. Gardner, A Novel 2D Vascular Network in Cementitious Materials, *Concr. – Innov. Des. Fib Symp. Copenhagen May 18-20, 2015 A.* (2015) 1–7. doi:10.1177/1753193414554772.
- [34] S. Pareek, K.C. Shrestha, Y. Suzuki, T. Omori, R. Kainuma, Y. Araki, Feasibility of externally activated self-repairing concrete with epoxy injection network and Cu-Al-Mn superelastic alloy reinforcing bars, *Smart Mater. Struct.* 23 (2014). doi:10.1088/0964-1726/23/10/105027.
- [35] P. Minnebo, G. Thierens, G. De Valck, K. Van Tittelboom, N. De Belie, D. Van Hemelrijck, E. Tsangouri, A novel design of autonomously healed concrete: Towards a vascular healing network, *Materials (Basel)*. 10 (2017) 1–23. doi:10.3390/ma10010049.
- [36] S. Sangadji, E. Schlangen, Self healing of concrete structures - novel approach using porous network concrete, *Journal of Advanced Concrete Technology*. 10 (2012) 185-194
- [37] L. Ferrara, T. Van Mullem, M.C. Alonso, P. Antonaci, R.P. Borg, E. Cuenca, A. Jefferson, P.L. Ng, A. Peled, M. Roig-Flores, M. Sanchez, C. Schroefl, P. Serna, D. Snoeck, J.M. Tulliani, N. De Belie, Experimental characterization of the self-healing capacity of cement based materials and its effects on the material performance: A state of the art report by COST Action SARCOS WG2, *Constr. Build. Mater.* 167 (2018) 115–142. doi:10.1016/j.conbuildmat.2018.01.143.
- [38] A. Sidiq, R. Gravina, F. Giustozzi, Is concrete healing really efficient? A review, *Constr. Build. Mater.* 205 (2019) 257–273. doi:10.1016/j.conbuildmat.2019.02.002.
- [39] C. Xue, W. Li, J. Li, V.W.Y. Tam, G. Ye, A review study on encapsulation-based self-healing for cementitious materials, *Struct. Concr.* 20 (2019) 198–212. doi:10.1002/suco.201800177.
- [40] T. Selvarajoo, R.E. Davies, B.L. Freeman, A.D. Jefferson, Characterisation of a vascular self-healing cementitious material system: mechanical healing, Submitted to *Construction and Building Materials*
- [41] E. Gruyaert, D. Debbaut, D. Snoeck, P. Díaz, A. Arizo, E. Tziviloglou, E. Schlangen, N. De Belie, Self-healing mortar with pH-sensitive superabsorbent polymers: testing of the sealing efficiency by

water flow tests, *Smart Materials and Structures* 25 (084007) (2016) 11, <https://doi.org/10.1088/0964-1726/25/8/084007>.

[42] D. Homma, H. Mihashi, T. Nishiwaki, Self-healing capability of fibre reinforced cementitious composites, *J. Adv. Concr. Technol.* 7 (2) (2009) 217–228, <https://doi.org/10.3151/jact.7.217>.

[43] M. Roig-Flores, S. Moscato, P. Serna, L. Ferrara, Self-healing capability of concrete with crystalline admixtures in different environments, *Constr. Build. Mater.* 86 (2015) 1–11, <https://doi.org/10.1016/j.conbuildmat.2015.03.091>.

[44] M. Roig Flores, F. Pirritano, P. Serna Ros, L. Ferrara, Effect of crystalline admixtures on the self-healing capability of early-age concrete studied by means of permeability and crack closing tests, *Constr. Build. Mater.* 114 (2016) 447–457, <https://doi.org/10.1016/j.conbuildmat.2016.03.196>.

[45] C. Edvardsen, Water Permeability and Autogenous Healing of Cracks in Concrete, *ACI Mater. J.* 96 (1999) 448–454.

[46] M. De Rooij, K. Van Tittelboom, N. De Belie, E. Schlangen, Self-healing Phenomena in Cement-Based Materials: State-of-the-art Report of RILEM Technical Committee 221-SHC: Self-Healing Phenomena in Cement-Based Materials, vol. 11, Springer, 2013.

[47] B.B. Sabir, S. Wild, M. O'Farrell, A water sorptivity test for mortar and concrete, *Mater. Struct.* 31 (1998) 568–574. doi:10.1007/BF02481540.

[48] M. Şahmaran, S.B. Keskin, G. Ozerkan, I.O. Yaman, Self-healing of mechanically-loaded self consolidating concretes with high volumes of fly ash, *Cem. Concr. Compos.* 30 (2008) 872–879. doi:10.1016/j.cemconcomp.2008.07.001.

[49] S. Jacobsen, J. Marchand, L. Boisvert, Effect of cracking and healing on chloride transport in OPC concrete, *Cement and Concrete Research.* 26 (1996) 869-881

[50] A. Darquennes, K. Olivier, F. Benboudjema, R. Gagné, Self-healing at early-age, a way to improve the chloride resistance of blast-furnace slag cementitious materials, *Constr. Build. Mater.* 113 (2016) 1017–1028, <https://doi.org/10.1016/j.conbuildmat.2016.03.087>.

[51] D. Gardner, A. Jefferson, A. Hoffman, R. Lark, Simulation of the capillary flow of an autonomic healing-agent in discrete cracks in cementitious materials, *Cem. Concr. Res.* 58 (2014) 35–44. doi:10.1016/j.cemconres.2014.01.005.

[52] D. Gardner, D. Herbert, M. Jayaprakash, A. Jefferson, A. Paul, Capillary Flow Characteristics of an Autogenic and Autonomic Healing-agent for Self-Healing Concrete, *J. Mater. Civ. Eng.* 29 (2017) 04017228. doi:10.1061/(ASCE)MT.1943-5533.0002092.

[53] K. Van Tittelboom, D. Snoeck, P. Vontobel, F.H. Wittmann, N. De Belie, Use of neutron radiography and tomography to visualize the autonomous crack sealing efficiency in cementitious materials, *Mater. Struct. Constr.* 46 (2013) 105–121. doi:10.1617/s11527-012-9887-1.

[54] T. Jefferson, E. Javierre, B. Freeman, A. Zaoui, E. Koenders, L. Ferrara, Research Progress on Numerical Models for Self-Healing Cementitious Materials, *Adv. Mater. Interfaces.* 5 (2018) 1–19. doi:10.1002/admi.201701378.

- [55] Cyanotec, Technical Data Sheet for Procure PC20. [http://www.gluesdirect.co.uk/catalog/product\\_info.php?products\\_id=151](http://www.gluesdirect.co.uk/catalog/product_info.php?products_id=151), 2016 (accessed 5 January 2019).
- [56] D. Gardner, A. Jefferson, A. Hoffman, Investigation of capillary flow in discrete cracks in cementitious materials, *Cem. Concr. Res.* 42 (2012) 972–981. doi:10.1016/j.cemconres.2012.03.017.
- [57] B. L. Karihaloo, *Fracture mechanics and structural concrete*, Longman Scientific & Technical, New York, 1995.
- [58] J. C. W. van Mier, *Fracture Processes of Concrete*, first ed., CRC Press, London, 1997.
- [59] J. A. Collins, K. C. Pani, R. A. Lehman, F. Leonard, Biological Substrates and Cure Rates of Cyanoacrylate Tissue Adhesive, *Arch. Surg.* 93 (1966) 428-432. doi:10.1001/archsurg.1966.01330030058013.
- [60] J. Comyn, Moisture cure of adhesives and sealants, *Int. J. Adhes. Adhes.* 18 (1998) 247–253. doi:10.1016/S0143-7496(97)00031-6.
- [61] S.K. Tomlinson, O.R. Ghita, R.M. Hooper, K.E. Evans, The use of near-infrared spectroscopy for the cure monitoring of an ethyl cyanoacrylate adhesive, *Vib. Spectrosc.* 40 (2006) 133–141. doi:10.1016/j.vibspec.2005.07.009.
- [62] T.D. Blake, The physics of moving wetting lines, *J. Colloid Interface Sci.* 299 (2006) 1–13. doi:10.1016/j.jcis.2006.03.051.
- [63] D.R. Gardner, R.J. Lark, B. Barr, Effect of conditioning temperature on the strength and permeability of normal- and high-strength concrete, *Cem. Concr. Res.* 35 (2005) 1400–1406. doi:10.1016/j.cemconres.2004.08.012.
- [64] A. M. Neville, *Properties of Concrete*, fifth ed., Prentice Hall, London, 2012.
- [65] Y.A. Villagrán Zaccardi, N.M. Alderete, N. De Belie, Improved model for capillary absorption in cementitious materials: Progress over the fourth root of time, *Cem. Concr. Res.* 100 (2017) 153–165. doi:10.1016/j.cemconres.2017.07.003.
- [66] C. Hall, W.D. Hoff, Rising damp: capillary rise dynamics in walls, *Proc. R. Soc. A.* 463 (2007) 1871-1884. doi:10.1098/rspa.2007.1855
- [67] A.S. Chitez, A.D. Jefferson, A coupled thermo-hygro-chemical model for characterising autogenous healing in ordinary cementitious materials, *Cem. Concr. Res.* 88 (2016) 184–197. doi:10.1016/j.cemconres.2016.07.002.
- [68] T. Jiang, S. Oh, J. C. Slattery, Correlation for dynamic contact angle, *J. Colloid Interface Sci.* 69 (1979) 74-77. doi:10.1016/0021-9797(79)90081-X.
- [69] M. Bracke, F. De Voeght, P. Joos, The kinetics of wetting: the dynamic contact angle, *Prog. Colloid Polym. Sci.* 79 (1989) 142-149.
- [70] R. G. Cox, The dynamics of the spreading of liquids on a solid surface. Part 1. Viscous flow, *J. Fluid Mech.* 168 (1986) 169-194. doi:10.1017/S0022112086000332.

- [71] A. F. Stalder, G. Kulik, D. Sage., L. Barbieri, P. Hoffmann, A snake-based approach to accurate determination of both contact points and contact angles, *Colloids and Surfaces A*. 286 (2006) 92-103. doi:10.1016/j.colsurfa.2006.03.008.
- [72] Biomedical Imaging Group, Drop Snake Analysis. <http://bigwww.epfl.ch/demo/dropanalysis/>, 2013 (accessed 15 October 2018).
- [73] N. Slepickova Kasalkova, P. Slepicka, Z. Kolska, V. Svorcik, Wettability and other surface properties of modified polymers, *Wetting and Wettability*. (2015) 324-352
- [74] A.M. Schwartz, S.B. Tejada, Studies of dynamic contact angles on solids, *Journal of Colloid and Interface Science*. 2 (1972) 359-375. doi:10.1016/0021-9797(72)90252-4
- [75] J.E. Seebergh, J.C. Berg, Dynamic wetting in the low capillary number regime, *Chemical Engineering Science*. 47 (1992) 4455-4464
- [76] B. L. Freeman, T. Jefferson. The simulation of transport processes in cementitious materials with embedded healing systems. *International Journal for Numerical and Analytical Methods in Geomechanics* (2019) <https://doi.org/10.1002/nag.3017>.
- [77] Z.P. Bažant, L.J. Najjar, Nonlinear water diffusion in nonsaturated concrete, *Matériaux Constr.* 5 (1972) 3–20. doi:10.1007/BF02479073.